Rotational Intermittency and Turbulence Induced Lift Experienced by Large Particles in a Turbulent Flow

Robert Zimmermann, Yoann Gasteuil, Mickael Bourgoin, Romain Volk, Alain Pumir, and Jean-François Pinton

Laboratoire de Physique de l'École Normale Supérieure de Lyon, UMR5672, CNRS and Université de Lyon, 46 Allée d'Italie, 69007 Lyon, France

(Received 17 December 2010; published 11 April 2011)

The motion of a large, neutrally buoyant, particle freely advected by a turbulent flow is determined experimentally. We demonstrate that both the translational and angular accelerations exhibit very wide probability distributions, a manifestation of intermittency. The orientation of the angular velocity with respect to the trajectory, as well as the translational acceleration conditioned on the spinning velocity, provides evidence of a lift force acting on the particle.

DOI: 10.1103/PhysRevLett.106.154501 PACS numbers: 47.27.T−, 05.60.Cd, 47.27.Ak, 47.55.Kf

The description of a solid object freely advected in a fluid requires, in addition to its translational degrees of freedom characterizing its position, 3 rotational degrees of freedom, specifying its orientation with respect to a reference frame. The evolution of its position and of its orientation depends, according to Newton's laws, on the forces and torques acting on the particle, which result from its interaction with the turbulent flow. Their determination raises challenging issues. The problem has been solved to a large extent for spherical particles of size D much smaller than the smallest length scale of the flow, the Kolmogorov scale η [1,2]. Because of the small size of the particle, the flow around it is locally laminar (see Fig. 1), so the equation governing the particle velocity $\boldsymbol{v}$ can be determined by solving the fluid (Stokes) equations once the fluid velocity $\boldsymbol{u}$ is known. In the simplest case, the particles are subject to the Stokes drag and the added mass term [3], so the velocity $\boldsymbol{v}$ can be determined by solving a simple differential equation. For $D \to 0$, the velocity of a neutrally buoyant particle reduces to the fluid velocity $\boldsymbol{u}$, so the particle behaves as a fluid tracer. This property is crucial for several experimental techniques [4]. In the limit $D \to 0$ [1,2], the translational and rotational degrees of freedom completely decouple.

Figure 1 suggests that the case of particles of radius larger than η is conceptually much more difficult. Experiments have shown that, upon increasing the ratio D/η from 1 to 40, the variance of the particle acceleration (i.e., of the forces) decreases as $(D/\eta)^{-2/3}$ [5,6]. The fluctuations of force remain non-Gaussian up to $D/\eta \lesssim 40$ [7–9], and a full derivation of the equation of motion of a large particle is still not available. The hydrodynamics forces can be decomposed parallel and perpendicular to the relative velocity $\mathbf{v}_{\mathrm{rel}}$ of the particle with respect to the flow. A generalization of the Magnus force, as derived in an inviscid, laminar flow: $\boldsymbol{F}_{\mathrm{lift}} = C_{\mathrm{lift}} \boldsymbol{v}_{\mathrm{rel}} \times \boldsymbol{\omega}^{\mathbb{P}}$, where $\boldsymbol{\omega}^{\mathbb{P}}$ is the rotation of the particle in the flow, appears as a natural possibility of a force acting perpendicular to $\boldsymbol{v}_{\mathrm{rel}}$ [10,11]. A lift has indeed been measured in laboratory experiments, when the flow is steady and laminar [12–14]. The flow conditions in these experiments are very different from the case of a particle in turbulence, schematically represented in Fig. 1. In such a flow field, the very definition of the fluid velocity around the particle is in fact very ambiguous. We therefore reduce the expression for the lift (Magnus) force to $\propto \boldsymbol{v} \times \boldsymbol{\omega}^{\mathbb{P}}$, where $\boldsymbol{v}$ is the particle velocity. The very existence of any lift force in these conditions, leading to a coupling between the translational and rotational degrees of freedom, is thus not obvious.

Here, we measure simultaneously the translational and rotational motion of a neutrally buoyant spherical particle, whose diameter is a fraction of the integral scale of the turbulence, and report the evidence of a lift force. We first briefly describe our six-dimensional tracking technique [15,16] and then present our results concerning the intermittency of the translational *and* rotational velocity and acceleration. Last, we discuss how the translational and rotational degrees of freedom of the particle couple, resulting in a lift force.

The flow and the tracking technique are described in detail in Ref. [16]. A von Kármán flow, as widely used for turbulence studies [6,17,18], is generated in the gap

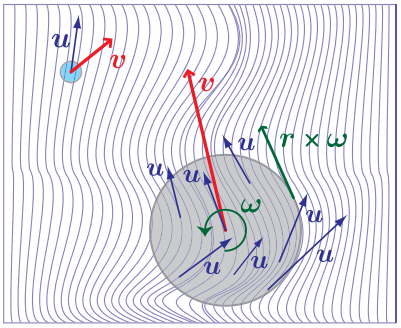

FIG. 1 (color online). Sketch of particles of increasing sizes superimposed on local velocity gradients. Whereas the flow around the small particle is smooth, it exhibits significant spatial variations around the large particle.

between two counterrotating impellers; see Fig. 2(a). In order to be able to perform direct optical measurements, the container is built with flat Plexiglas side walls, so that the cross section of the vessel has a square shape.

The driving disks are rotated here at 3 Hz, corresponding to an energy injection rate of $\varepsilon \sim 1.7$ W/kg. The integral time and length scales are $L_{\rm int} = 3$ cm and $T_L = 0.3$ s, respectively, so that the dissipative length and time scales are, respectively, $\eta \sim 30$ μm and $\tau_\eta \sim 1$ ms. The flow Reynolds number based on the Taylor microscale is $R_\lambda \sim 300$.

A polyamide sphere with density $\rho_p = 1.14$ g $\cdot$ cm^{-3} and diameter $D = 18$ mm is made neutrally buoyant by adjusting the density of the fluid by addition of glycerol to water (the final density mismatch is less than $\Delta\rho/\rho = 10^{-4}$). The spheres are homogeneous; i.e., the particle center of mass coincides with its geometrical center. Their size is comparable to the integral length of the flow, corresponding to $D/\eta \sim 600$ and $D/L_{\rm int} \sim 0.6$. Its motion is recorded at 600 Hz, by using 2 high-speed video cameras (Phantom V12, Vision Research Inc.) positioned at 90°. The measurement volume lies within 75% of the radial and axial distances on either side of the flow center, i.e., extends to regions where anisotropy and inhomogeneity are known to play a role. Restricting the measurement volume closer to the center does not affect significantly our results, thus strongly suggesting that the effects discussed in this Letter are not artifacts of the experimental setup. The position of the sphere is determined by using a position tracking algorithm, as in Ref. [6]. The time-resolved determination of the rotational degrees of freedom [15,16] is carried out by painting a pattern that enables a determination of the particle's orientation from the camera images; cf. Fig. 2(c). The orientation tracking algorithm then (i) compares the sphere's picture with synthetic images and identifies a set of possible orientations; (ii) from the set of possible candidates at successive instants, a *flow* algorithm identifies a likely time series; and (iii) a posttreatment adjusts remaining ambiguities, by using the independent views from the 2 cameras. After processing, all trajectories with a duration longer than $0.25T_L$ are analyzed, leaving 3434 trajectories with duration ranging between 0.25 and $3T_L$. A few particular examples are shown in Fig. 2(d), showing the position, color coded for the amplitude of the acceleration, together with two unit vectors fixed in the reference frame of the particle. Velocity and acceleration are computed from convolution with Gaussian kernels, as described in Refs. [16,19].

We find that the behavior of the translational degrees of freedom is qualitatively very similar to the results obtained for much smaller particles [5,7–9]—the size of the particles studied so far did not exceed $D \lesssim 40\eta$, whereas ours has $D \approx 600\eta$. The particle velocity has a quasi-Gaussian distribution; each component has zero mean and an rms intensity of fluctuations of about 60 cm/s, for impellers rotating at 3 Hz. This is of the order of 30% of the impeller tip speed and also of the order of the rms velocity fluctuations of tracers in the same flow. This leads to the consistent notion that the velocities of the particle are of the order of the large scale swirls generated in the von Kármán setup. The particle Reynolds number $\mathrm{Re}_p \equiv u_{\rm rms} D/\nu$ is estimated to $\sim$1200; one expects that the Reynolds number *relative* to the local fluid motions is of the same order of magnitude.

The particle's acceleration, with zero mean, has an rms amplitude of fluctuations equal to 8.5 m/s^2. Its probability distribution function (PDF) has strongly non-Gaussian fluctuations; see Fig. 3. In terms of velocity increments, the acceleration can be viewed as a velocity change over the shortest time scale, while the velocity increments over long times scales have the same distribution as the velocity itself. We have checked that, as expected, the PDFs of velocity increments evolve smoothly from a shape with wide tails [19] for very small time lags to a Gaussian shape

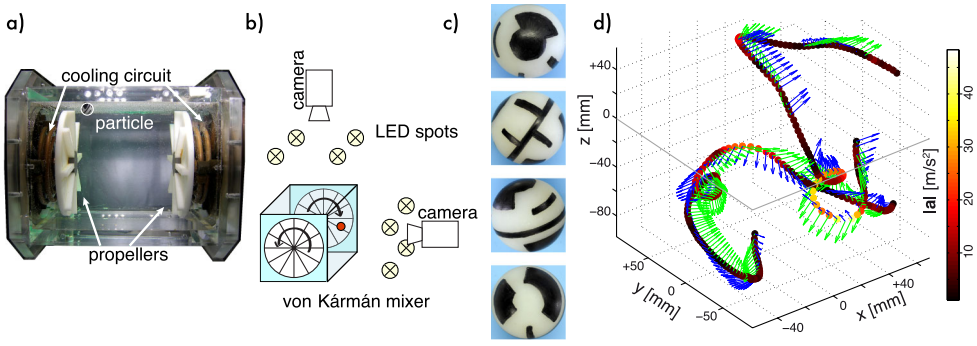

FIG. 2 (color online). (a) The flow domain in between the impeller has characteristic lengths $H = 2R = 20$ cm; the disks have radius $R = 10$ cm, fitted with straight blades 1 cm in height. (b) It is illuminated by high power light-emitting diodes, and sequences of 8-bit gray-scale images are recorded by using high-speed cameras; (c) an adequate texture painted on the particle allows the tracking of its orientation; (d) example of particle tracks and orientations (the green and blue arrows mark North-South and East-West directions, respectively).

at long time intervals, a phenomenon often called intermittency. This effect is observed here for a very large particle, compared to the Kolmogorov scale, η. The strong events in the acceleration PDF are, however, less intense than in the case of smaller particles. We estimate the normalized fourth moment, the flatness, to be $F = 7 \pm 1$ for our particle with $D/L_{\rm int} \sim 0.6$. Remarkably, this value is identical to the one found in Ref. [7], with a comparable ratio $D/L_{\rm int} \lesssim 1$, and generally with the very slow decay of the flatness with D observed in Refs. [9,20] for particles much smaller compared to $L_{\rm int}$ ($D/L_{\rm int} \sim 1/50$).

We now turn to the angular velocity of the sphere, $\boldsymbol{\omega}^{\mathbb{P}}$. The three components fluctuate around a zero mean value, with no preferred orientation, and their rms amplitude is 12 rad/s. This value is comparable to the rotation rate of the driving disks and also corresponds to the rotation that would result from imposing a velocity difference of the order of $u_{\rm rms}$ across the particle diameter D ($u_{\rm rms}/D \simeq$ 30 rad/s). The PDFs of angular velocity components are shown in Fig. 3. The distributions are symmetric and slightly non-Gaussian (we estimate a flatness $F \sim 4$). The rms amplitude of the angular acceleration $\boldsymbol{\alpha}^{\mathbb{P}}$ is about 700 rad/s^2, again of the order of $(u_{\rm rms}/D)^2$. The PDF of $\boldsymbol{\alpha}^{\mathbb{P}}$ is strongly non-Gaussian (we estimate $F = 7 \pm 1$). Hence, the PDFs of the angular velocity increments become broader when the time lag τ decreases from $\tau \sim T_L$ to $\tau \sim \tau_\eta$: The angular dynamics is intermittent.

We now address the question of the coupling between the dynamics of rotation and translation. Figure 4(a) reveals a strong alignment between the direction of the angular velocity $\boldsymbol{\omega}^{\mathbb{P}}$ and the vectors defining the trajectory—the usual Frenet coordinate system ($\boldsymbol{T}$, $\boldsymbol{N}$, $\boldsymbol{B}$), denoting, respectively, the units vectors along the velocity, the curvature, and the direction perpendicular to the tangent plane of the trajectory. The fairly sharp distribution of the direction of $\boldsymbol{\omega}^{\mathbb{P}}$ on the sphere is quite surprising.

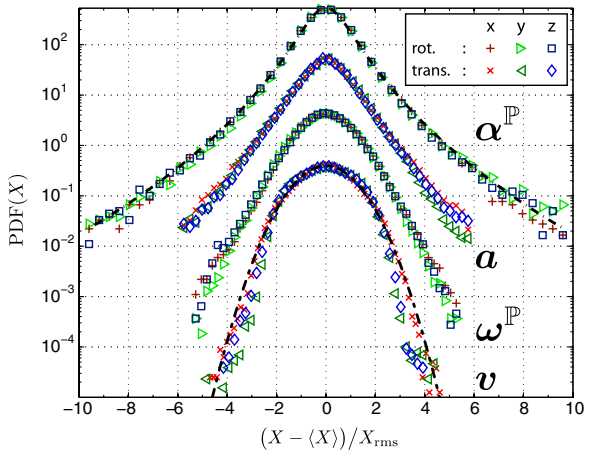

FIG. 3 (color online). PDFs of velocity and acceleration, for the linear and angular motions. The curves have been shifted vertically for clarity.

In fact, Fig. 4(a) shows a maximum of probability at an angle of the order of 45° with respect to $\boldsymbol{T}$ in the ($\boldsymbol{T}$, $\boldsymbol{B}$) plane. This effective breaking of the rotational symmetry of $\boldsymbol{\omega}^{\mathbb{P}}$ strongly suggests a coupling between the translational and the rotational dynamics. We also note that $\boldsymbol{\omega}^{\mathbb{P}}$ is aligned perpendicular to $\boldsymbol{N}$, so both the acceleration $\boldsymbol{a}$ and $\boldsymbol{v} \times \boldsymbol{\omega}^{\mathbb{P}}$ lie in the ($\boldsymbol{T}$, $\boldsymbol{N}$) plane. Our measurements thus demonstrate that the expected expression of the lift (Magnus) force, $\approx \boldsymbol{v} \times \boldsymbol{\omega}^{\mathbb{P}}$, has a strong component in the $\boldsymbol{N}$ direction. This is consistent with a lift force acting on the particle. Further evidence for a lift force is provided by the observation that the amplitude of the normal acceleration, $a_N \equiv \boldsymbol{a} \cdot \boldsymbol{N}$, conditioned on the amplitude of $\omega_B \equiv \boldsymbol{\omega}^{\mathbb{P}} \cdot \boldsymbol{B}$ [Fig. 4(b)] increases from 6 to 9 m/s^2 (half a standard deviation) when the particle rotation varies in the range ± 12 rad/s (i.e., 1 standard deviation in rotation speed).

The main results of this work concern the strong intermittency for both the translational and the rotational accelerations and the coupling between the rotational and translational degrees of freedom.

The observed intermittency of the translational and rotational accelerations points to very intense fluctuations of the force and torque acting on the particle. The interaction between the sphere and the flow involves a pressure and a viscous term, resulting from the stress tensor:

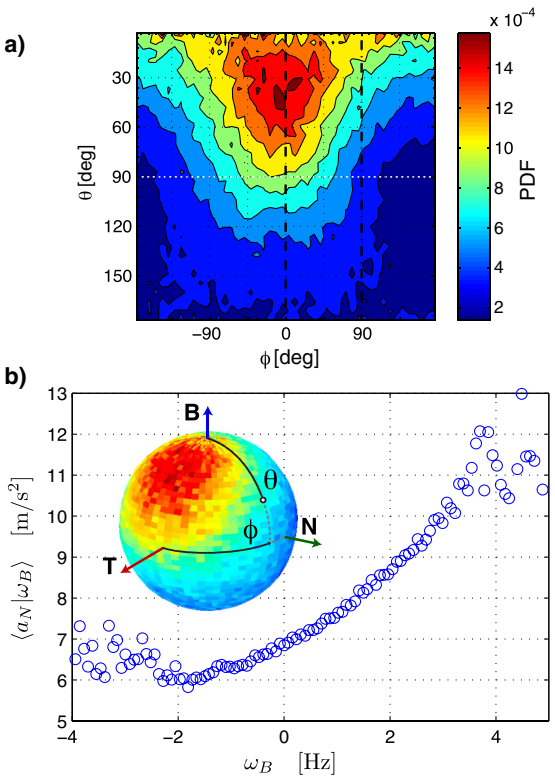

FIG. 4 (color online). (a) Alignment of the angular velocity $\boldsymbol{\omega}^{\mathbb{P}}$ with respect to the moving Frenet coordinate system; (b) normal acceleration conditioned to the component of angular velocity parallel to the binormal Frenet vector.

$\tau_{ij} = -p\delta_{ij} + \rho\nu(\partial_i u_j + \partial_j u_i)$. Measurements of the drag force acting on a particle of a large Reynolds numbers [21] demonstrate that pressure is the dominant effect in the force: At the particle Reynolds number in our experiment, $\mathrm{Re}_P \approx 10^3$, friction contributes to ~20% of the drag; this fraction diminishes at higher Reynolds numbers. Pressure is expected to be mostly coherent at the scale of our particle $D \sim L$, so the pressure effects act collectively on the object, resulting in a force of order $\rho D^2 u_{\mathrm{rms}}^2$, which yields the correct order of magnitude for the rms of the particle acceleration. The strongly non-Gaussian PDFs of $\boldsymbol{a}$ are more surprising, since the force acting on the particle results from an averaging over a size comparable to the correlation length of the flow.

The effect of friction, although weak compared to pressure, is essential to understand the torque. In fact, the pressure force, perpendicular to the surface of the sphere, does not contribute to the torque applied at the center of the particle. Thus, the rms of the angular acceleration is $\langle(\boldsymbol{\alpha}^{\mathbb{P}})^2\rangle^{1/2} \sim \langle\Gamma_v^2\rangle^{1/2}/I$, where Γ_v is the torque and I the moment of inertia of the particle. The torque results from an integral over the particle's surface, and Γ_v is proportional to $\nu\partial_x u$. This viscous term is quantified by the skin friction velocity $u_*^2 \equiv \nu\partial_x u$. Given the weak value of the moment of inertia $I = MD^2/10$, where M is the mass of the particle, one obtains $\langle(\boldsymbol{\alpha}^{\mathbb{P}})^2\rangle^{1/2} \sim 10(u_*/D)^2$. Previous measurements suggest a ratio u_*^2/u_{rms}^2 of the order of 0.2 at the particle Reynold's number $\mathrm{Re}_p \approx 1000$ [21]. This leads to $\langle(\boldsymbol{\alpha}^{\mathbb{P}})^2\rangle \sim (u_{\mathrm{rms}}^2/D^2)^2$, as observed in our experiment. Which properties of the turbulent flow control the rate of rotation of the particle also remains to be elucidated. In this respect, the naive vision of many small eddies, compared to the size of our big particle, implicit in Fig. 1, is likely to be an oversimplification. Small eddies acting on the particle in a spatially incoherent manner would result in a significantly reduced torque acting on the particle. This suggests a much more coherent flow pattern, at least at our particle Reynolds numbers, in fact consistent with the recent numerical results of Ref. [22]. We also note that, while the estimates above provide a qualitative explanation of the observed velocities and accelerations rms values, understanding the complete statistics of their fluctuations remains a challenge. Our evidence of a lift effect, i.e., a strong coupling between rotation and translation, rests on conditioning the acceleration (force) on the angular velocity of the particle, $\boldsymbol{\omega}^{\mathbb{P}}$. While this is a very sensible choice, the actual torque acting on the particle depends on the local structure of the flow, which remains to be determined, for instance, by local particle image (or tracking) velocimetry around the moving sphere [23] or numerically [20,22,24]. The sharply peaked distribution of $\boldsymbol{\omega}^{\mathbb{P}}$ in the Frenet basis [see Fig. 4(a)] is a very surprising result of this work. In this respect, determining experimentally the variation of the quantities studied here as a function of particle size and Reynolds number should provide important clues on the interaction between turbulent flow and the particle.

This work is part of the International Collaboration for Turbulence Research. We thank Aurore Naso for many fruitful discussions. This work was supported by ANR-07-BLAN-0155 and by PPF "Particules en Turbulence" from the Université de Lyon.

[1] R. Gatignol, J. Mec. Theor. Appl. **2**, 143 (1983).
[2] M. R. Maxey and J. J. Riley, Phys. Fluids **26**, 883 (1983).
[3] S. Elghobashi and G. C. Truesdell, J. Fluid Mech. **242**, 655 (1992).
[4] *Handbook of Experimental Fluid Dynamics* (Springer, New York, 2007).
[5] N. M. Qureshi *et al.*, Phys. Rev. Lett. **99**, 184502 (2007).
[6] G. A. Voth *et al.*, J. Fluid Mech. **469**, 121 (2002).
[7] N. M. Qureshi *et al.*, Eur. Phys. J. B **66**, 531 (2008).
[8] R. D. Brown, Z. Warhaft, and G. A. Voth, Phys. Rev. Lett. **103**, 194501 (2009).
[9] R. Volk *et al.*, J. Fluid Mech. **668**, 223 (2011).
[10] T. R. Auton, J. C. R. Hunt, and M. Prud'homme, J. Fluid Mech. **197**, 241 (1988).
[11] E. Loth and A. J. Dorgan, Environ. Fluid Mech. **9**, 187 (2009).
[12] J. Ye and M. Roco, Phys. Fluids A **4**, 220 (1992).
[13] E. A. van Nierop *et al.*, J. Fluid Mech. **571**, 439 (2007).
[14] M. Rastello *et al.*, J. Fluid Mech. **624**, 159 (2009).
[15] Y. Gasteuil, Ph.D. thesis, ENS Lyon, 2009.
[16] R. Zimmermann *et al.*, Rev. Sci. Instrum. **82**, 033906 (2011).
[17] R. Monchaux *et al.*, Phys. Rev. Lett. **96**, 124502 (2006).
[18] N. T. Ouellette *et al.*, New J. Phys. **8**, 109 (2006).
[19] N. Mordant, A. M. Crawford, and E. Bodenschatz, Physica (Amsterdam) **193D**, 245 (2004).
[20] H. Homann and J. Bec, J. Fluid Mech. **651**, 81 (2010).
[21] E. Achenbach, J. Fluid Mech. **54**, 565 (1972).
[22] A. Naso and A. Prosperetti, New J. Phys. **12**, 033040 (2010).
[23] M. Gibert and E. Bodenschatz (private communication).
[24] F. Lucci, A. Ferrante, and S. Elghobashi, J. Fluid Mech. **650**, 5 (2010).